Journal of Sound and Vibration (1998) **218**(2), 269–292
Article No. sv981832

UNIVERSAL BUMPERED VIBRATION ISOLATOR FOR SEVERE ENVIRONMENT

V. I. Babitsky and A. M. Veprik†

*Department of Mechanical Engineering, Loughborough University, Leicestershire LE*11 3*TU, England*

(*Received* 27 *October* 1997, *and in final form* 22 *June* 1998)

Modern compact design often does not permit the effective use of linear vibration isolation in the case of the intense environmental disturbances. Demands for limitation of the dynamic deflections lead to the use of heavy damped vibration isolators, sometimes in combination with the bumpers installed with the maximal free travel. The increase in isolator damping improves the low frequency resonant response at the expense of an inferior isolation performance in the high-frequency range. The installation of bumpers with enlarged travel reduces the probability of the accidental impacts and effectively trims the excessive deflections in an emergency. However, it turns the isolator into a vibro-impact structure, where the appearance of intense impulsive accelerations and high-powered non-linear resonance becomes the subject of concern. The idea of the present novel concept is based on co-operative use of an *undamped*, *low frequency vibration isolator* in combination with *optimally damped bumpers* installed with *minimal free travel*. Such an isolator demonstrates the advantages of the linear undamped isolator under low level ambient and operational high frequency excitation. However, under severe ambient disturbances, for any excessive deflections, it becomes strongly non-linear and takes on the quality of an optimal shock absorber. The approach formulated has been applied successfully to a design of a gimballed electro-optical device based on the linear split Sterling cryocooler for a focal array.

1. INTRODUCTION

The limiting of vibratory energy transmission from a machine to its foundation and *vice versa* may be achieved by the proper use of a flexural suspension. If the natural frequencies of the resiliently suspended machine are located well below the lowest frequency in the excitation spectrum, a significant attenuation of vibration transmission may be achieved in a certain high-frequency range. In this case, it is recommended to use a soft and undamped flexural suspension [1].

In fact, such a simple vibration isolator is feasible in a limited number of cases of moderate environmental disturbances. As soon as an application involves exposure to severe environmental disturbances such as shock or broadband

† Formerly Ricor Cyogenic & Vacuum Systems, En Harod Ihud 18960, Israel.

0022–460X/98/470269 + 24 $30.00/0

random vibration, the spectrum of excitation already contains dangerous low frequency components. The low frequency and undamped isolator under such conditions exhibits excessive deflections that can over-stress the flexural suspension and even damage the machine or its enclosure.

Due to the possible low frequency amplification, the flexible suspension must be supplied in this case with considerable free oscillation space to avert impacts against the machine enclosure [2]. Modern compact mechanical design, however, does not permit such a possibility. The constraint of the space together with the demands for the safety of the machine enclosure, resilient supports and a flexible interface necessitates close control of vibration amplification at quasi-resonance or at shock.

The most generic solution combines the increase of free travel of the vibration isolator (as is permitted by design) and the choice of the loss factor of the suspension with respect to the transmissibility ratio at the operational frequency.

It is considered that an optimal flexible suspension has a compromising loss factor of 0·3, thus providing resonance amplification of about 2, and 73% vibration isolation at a frequency which is four times that of the natural frequency. Increased free travel minimizes the probability of undesirable strike-through of vibration isolation and prevents the non-linear resonance appearance.

Such a design produces spacious, heavily damped vibration isolators, where a high loss factor of the resilient elements negates the quality of vibration isolation in a high-frequency range. Moreover, the increase in this loss factor cannot prevent the appearance of excessive deflections at ambient random vibration or at shock. In order to protect a machine and its enclosure from unavoidable excessive motions, the pre-designed deflection limiters—bumpers—are usually an integral component of a vibration isolation arrangement. If of sufficient stiffness, bumpers can effectively trim machine deflections in an emergency.

However, the presence of bumpers turns the vibration isolation arrangement into a potential strongly non-linear (vibro-impact) system with new, sometimes unfavourable, dynamic qualities [3]. Main or even sub-harmonic vibro-impact resonance in a frequency range located well above the system natural frequency may arise after casual vibration disturbance or frequency pulling at machine start-up. With the increase in free vibration space there exists the danger of the appearance of intense impulsive accelerations due to the development of large pre-impact velocities.

There is an attempt in this paper to revise the traditional approach to the design of bumpered vibration isolation arrangement. The low frequency and undamped vibration isolator with soft and heavily damped bumpers is considered as a tool for simultaneous control of vibration export and excessive deflections.

The special installation of the bumpers permits only a minimum of the free travel required for the impactless operation of the isolator when free of intense ambient disturbances. Under a low-level ambient and typical high frequency excitation, such a vibration isolator appears to be linear, undamped and highly responsive with excellent vibration isolation ratio in a high-frequency range.

Any excess of the pre-designed free travel due to the intense ambient disturbance results in a momentary generation of the impulsive restoring force of the bumper.

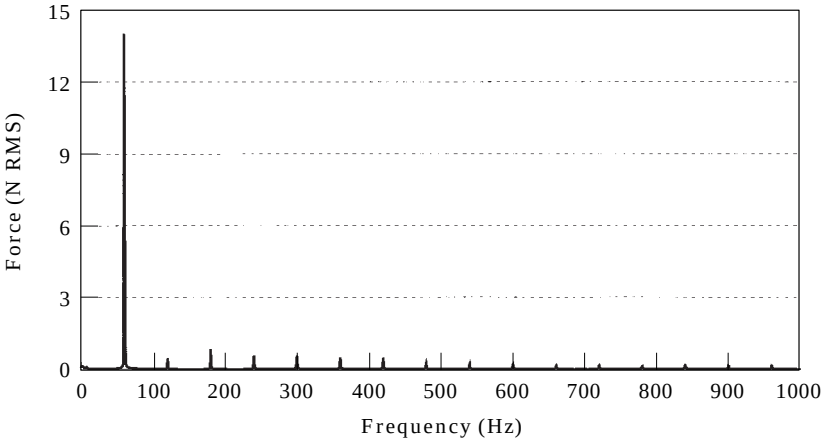

Figure 1. Spectral presentation of self-induced force of linear compressor.

Stiffness and damping obtained during the collision cause the quick halt of the isolator within a very short compression stroke and low rebound without generation of ruinous accelerations.

In this context, it became clear that the bumper has to be designed as an optimal shock absorber. Such parameters as free oscillation space, bumper stiffness and damping will be treated further as possible keys to the global improvement of quality of non-linear vibration protection systems.

2. DESCRIPTION OF A SPECIFIC APPLICATION

The typical case of a bumpered vibration protection arrangement as applied to a design of a gimballed electro-optical device [4] will be discussed. The above device was based on a split Sterling cryocooler (Ricor model K529H, consisting, respectively, of compressor and expander units) for the cooling of an infrared focal array.

The self-induced force†, produced by the operating compressor contains in its spectra an intense pure-frequency component 14 N RMS @ 60 Hz, as shown in Figure 1. It appeared to be the dominant disturbing factor of the specific gimballed electro-optical application. It was established experimentally that normal operation of precise optics might be achieved if the force produced by the compressor unit is less than 1 N RMS at the fundamental frequency. In order to achieve such an attenuation factor, an undamped low-frequency vibration isolator with natural frequency of 15 Hz and loss factor of 0·05 may be used (see, for instance, the curves of absolute transmissibility in reference [5]).

In the new arrangement (see Figure 2(a)) the compressor unit 1 was suspended from its base 2 by all-metal undamped planar soft resilient elements 3. Excessive motion of the compressor unit, originated by possible acceleration of the

† The measurement of the self-induced force was carried out with a Kistler Type 9272 Quartz four-component Dynamometer, Kistler Type 5010A Charge Conditioner and Scientific Atlanta Type SD-390 Signal Analyzer.

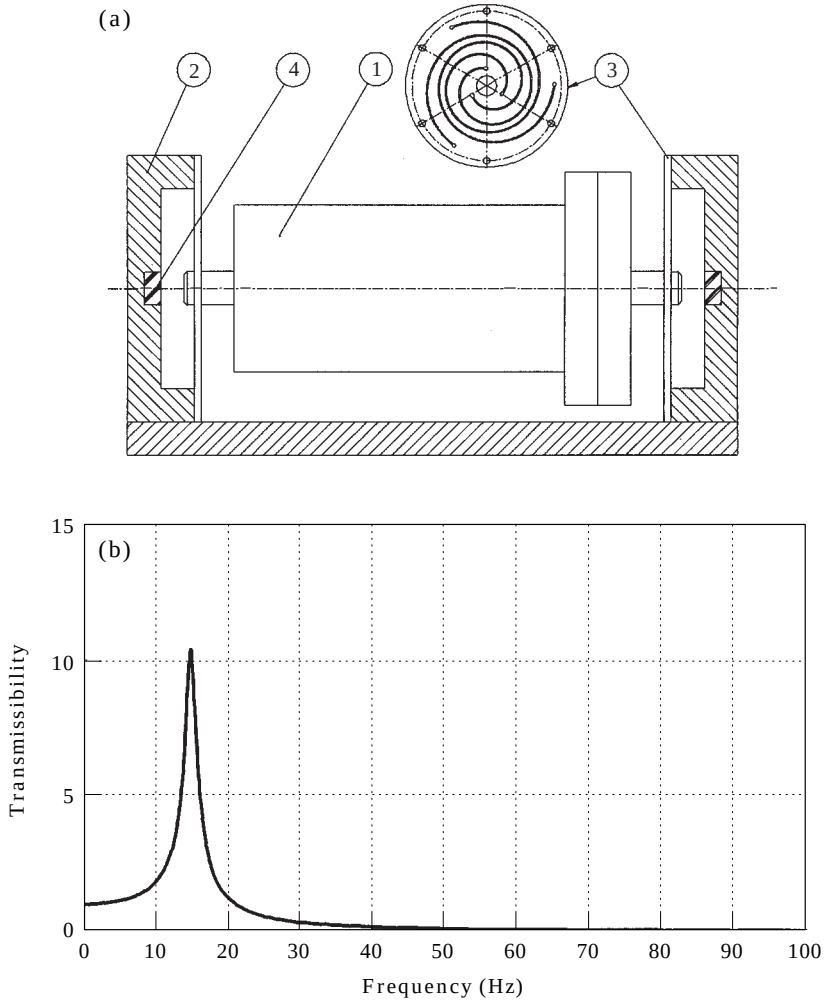

Figure 2. Vibration isolation arrangement (a) and transmissibility (b) for the linear compressor unit.

foundation, was limited by the elastomeric bumpers 4 mounted over the same foundation.

This arrangement provided a natural frequency of 15 Hz and loss factor of 0·05 (see the experimental transmissibility curve in Figure 2(b)). As a result, the fundamental component of self-induced force was reduced by up to 0·95 N RMS (see Figure 3(a)). The fundamental component of the dynamic deflection of the compressor unit was measured as 0·23 mm RMS, or a 0·35 mm peak (see Figure 3(b)).

To allow compressor operation without impacts in the absence of environmental disturbances, the clearance in between the compressor housing and the bumpers was chosen to be greater than the sum of the possible static deflection and the peak operational amplitude. Referring to the natural frequency of 15 Hz, one obtains

the maximum static deflection of ~ 1 mm. By adding the peak displacement of $\sim 0{\cdot}35$ mm (see Figure 3(b)) and small tolerance for safety, one has $\Delta = 1{\cdot}5$ mm.

Modern viscoelastic materials, composed of energy absorbing thermoplastic alloys, such as E-A-R Isodamp, are used widely for shock control. A typical application is motion limiters—bumpers—which provide low-rebound and soft trim of undesirable mechanical deflections without generation of dangerous accelerations. The design of the optimal bumpers requires a simple and reliable model of impact, allowing the exact estimation of the peak values of the impulsive acceleration and deflection.

3. MODEL OF VISCOELASTIC IMPACT

In the present section, the simplified model of single impact of a free lumped body over the "*Kelvin-Voigt*" bumper was considered. The analytical solution,

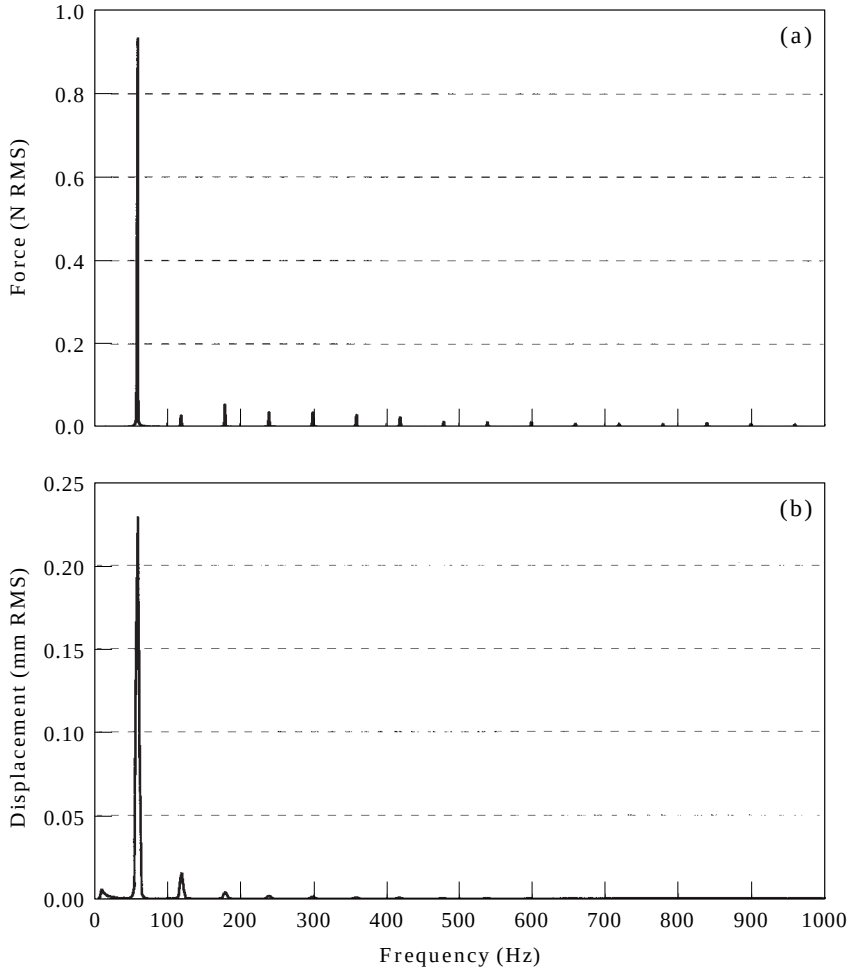

Figure 3. Spectral presentation of the transmitted force (a) and dynamic deflection (b) of the flexurally suspended compressor unit.

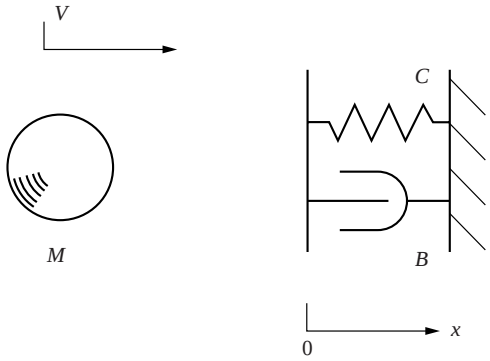

Figure 4. Model of viscoelastic impact.

describing the dynamics of impact, was obtained. The parameters of the optimal shock absorber were estimated. This solution was used further to verify experimentally the model of impact.

3.1. THEORETICAL CONSIDERATIONS

Figure 4 presents the model of axial collision of a free lumped body of mass M with the viscoelastic "*Kelvin-Voigt*" bumper. The bumper was modelled schematically as a parallel combination of linear spring K and dashpot B with "grounded" right-hand side terminals. Such a model accurately describes dynamic strain and deformation that occur in a viscoelastic sample under impulsive loading. The "*Kelvin-Voigt*" body prevents spontaneous response as the spring is constrained by the dashpot and, therefore, the strain and deformation under the load is controlled dynamically by the dashpot.

Dynamic balance between the force of bumper reaction $R = KX + B\dot{X}$ and the force of the body inertia $M\ddot{X}$ governs the development of collision. By equating the mentioned forces, one can obtain the differential equation of the impact—the equation of the cooperative motion of the body and the free terminal of the bumper,

$$M\ddot{X} + B\dot{X} + KX = 0, \qquad t \in [0, \alpha], \tag{1}$$

where α denotes the instant of the separation (rebound). The initial conditions for equation (1) are as follows: $X(0) = 0$, $\dot{X}(0) = V$. The condition of the body separation at $t = \alpha$ is the change of the sign of the force of bumper reaction or of the body acceleration:

$$R(\alpha) = 0 \qquad \text{or} \qquad \ddot{X}(\alpha) = 0. \tag{2}$$

The equation of impact (1) has a well-known solution,

$$X(t) = A \exp(-ht) \sin \Omega t, \qquad t \in [0, \alpha], \tag{3}$$

where the traditional notations are used:

$$h = B/2M, \qquad A = V/\Omega, \qquad \Omega^2 = \omega^2 - h^2, \qquad \omega^2 = K/M.$$

In fact, the damped and undamped natural frequencies Ω and ω, respectively, are the apparent quantities that are related to the mass of the body.

The corresponding derivatives with respect to time obtained from equation (3) are as follows:

$$\dot{X} = A \exp(-ht)(\Omega \cos \Omega t - h \sin \Omega t),$$

$$\ddot{X} = -A \exp(-ht)[(\Omega^2 - h^2) \sin \Omega t + 2h\Omega \cos \Omega t],$$

$$\dddot{X} = -A \exp(-ht)[(3h\Omega^2 - h^3) \sin \Omega t + (3h^2\Omega - \Omega^3) \cos \Omega t], \qquad t \in [0, \alpha]. \quad (4)$$

After solving equation (2) for the separation time α, one finds that

$$\alpha = \frac{1}{\Omega} \operatorname{atan} \frac{-2h\Omega}{\Omega^2 - h^2},$$

or with the notation for the fraction of critical damping (loss factor) $\xi = h/\omega$,

$$\alpha = -\frac{1}{\omega\sqrt{1 - \xi^2}} \operatorname{atan} \frac{2\xi\sqrt{1 - \xi^2}}{1 - 2\xi^2}. \quad (5)$$

The peak value of acceleration may occur at the very beginning of the collision (due to the immediate step-wise reaction force $R(0) = VB$) or at the time instant when $\dddot{X}(t) = 0$.

The value of the initial acceleration may be calculated by using the statement $M\ddot{X}_0 = R = VB$ from which it follows

$$\ddot{X}_0 = VB/M = 2V\xi\omega. \quad (6)$$

The maximum value of acceleration occurs in the time instant when $\dddot{X}(\vartheta) = 0$ ($\vartheta < \alpha$); therefore, upon considering the third-order derivative from equations (4), the instant of the acceleration peak may be found as

$$\vartheta = -\frac{1}{\omega\sqrt{1 - \xi^2}} \operatorname{atan} \frac{(4\xi^2 - 1)\sqrt{1 - \xi^2}}{\xi(3 - 4\xi^2)}. \quad (7)$$

By substituting the corresponding values of the time instant ϑ from equation (7) into the expression for the acceleration from equations (4) and after rearrangement the following maximum value has been obtained:

$$\ddot{X}_{max} = V\omega\gamma(\xi). \quad (8)$$

Here

$$\gamma(\xi) = \frac{1}{\xi(3 - 4\xi^2)} \exp\left[-\frac{\xi}{\sqrt{1 - \xi^2}} \operatorname{atan} \frac{(4\xi^2 - 1)\sqrt{1 - \xi^2}}{\xi(3 - 4\xi^2)}\right] \times \cos\left[\operatorname{atan} \frac{(4\xi^2 - 1)\sqrt{1 - \xi^2}}{\xi(3 - 4\xi^2)}\right].$$

Finally, combining equations (6) and (8) yields for the maximorum maximum

$$\hat{\ddot{X}} = V\omega\Gamma(\xi). \quad (9)$$

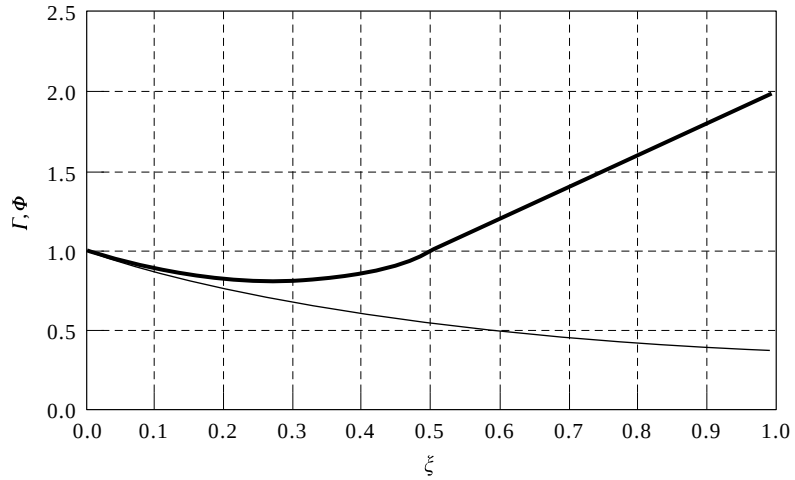

Figure 5. Values Γ (——) and Φ (——) at viscoelastic impact as functions of loss factor of the bumper.

Here

$$\Gamma(\xi) = \begin{Bmatrix} \gamma(\xi) & \text{if} & \gamma(\xi) \geqslant 2\xi \\ 2\xi & \text{if} & \gamma(\xi) < 2\xi \end{Bmatrix}. \tag{10}$$

The value of $\xi = 0{\cdot}5$ is the exact solution for the equation $\gamma(\xi) = 2\xi$. That means, that for the viscoelastic bumpers with $\xi > 0{\cdot}5$ the peak of acceleration occurs at the beginning of the collision.

The peak deflection occurs when $\dot{X}(\tau) = 0$ $(\tau < \alpha)$; therefore, with the help of expression for the first-order derivative from equations (4), the instant of maximum deflection may be found as

$$\tau = \left(\operatorname{atan} \frac{\sqrt{1-\xi^2}}{\xi} \right) \Big/ \left(\omega \sqrt{1-\xi^2} \right). \tag{11}$$

By substituting the corresponding values of the time instant τ from equation (11) into the expression for the deflection from equations (4) and after rearrangements the following peak value was obtained,

$$\hat{X} = (V/\omega)\Phi(\xi) \tag{12}$$

where

$$\Phi(\xi) = \frac{1}{\sqrt{1-\xi^2}} \exp\left[-\frac{\xi}{\sqrt{1-\xi^2}} \operatorname{atan} \frac{\sqrt{1-\xi^2}}{\xi} \right] \sin\left[\operatorname{atan} \frac{\sqrt{1-\xi^2}}{\xi} \right]. \tag{13}$$

Figure 5 depicts functions (13) and (10) superimposed†.

† This result is somewhat similar to that obtained in reference [1] for the maximum deflection and transmitted force for the SDOF vibration isolator under impulse excitation.

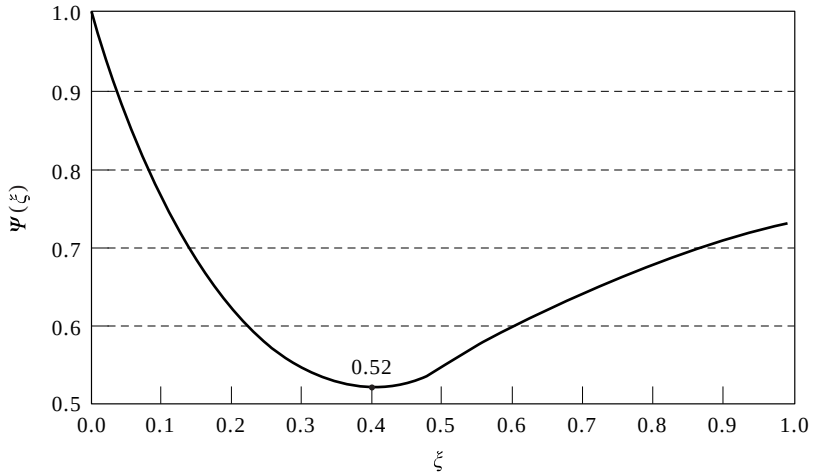

Figure 6. Optimization criterion at viscoelastic impact as a function of bumper loss function.

3.2. OPTIMIZATION OF IMPACT

As can be seen from equations (10) and (13), the peak value of deflection and acceleration depend upon the pre-impact velocity V, the apparent natural frequency ω and the loss factor ξ of the bumper.

But the product of the mentioned peak values,

$$\Pi = \hat{\dot{X}}\,\hat{X} = V^2\Psi(\xi), \tag{14}$$

where $\Psi(\xi) = \Gamma(\xi)\Phi(\xi)$, does not contain the factor ω. Figure 6 depicts the function $\Psi(\xi)$ approaching the minimum at $\xi = 0{\cdot}4$. Considering the factor Π as a vibration isolator quality [1], we conclude that the optimal loss factor equals 0·4 independent of the bumper stiffness and pre-impact velocity. For the optimal bumper, $\Psi_{opt} = \Psi(0{\cdot}4) = 0{\cdot}52$, as shown in Figure 6 and $\Pi = 0{\cdot}52V^2$. In comparison with the undamped bumper, the improvement will be about a 50% decrease of the chosen criterion.

3.3. EXPERIMENTAL VALIDATION OF THE MODEL

Figure 7 represents the experimental rig. The plastic pad (E-A-R Isodamp C-1000 plastic, 6·4 mm thickness) was mounted in a vice fixture with the plain surface facing the pendulum. The weighted, bifilary suspended steel rod (∅ 10 mm) with a radiused tip was fixed at a point directly above the sample vice. It was swung up and then held stationary. This height defined the approaching speed of the pendulum at impact. When released, the pendulum swings through the path where the sample was fixed.

The typical example of the development of obtained time history of acceleration is depicted in Figure 8†.

† The process of collision was registered by a Bruel & Kjaer miniature Accelerometer Type 4393 (mounted over the plane edge of the rod) along with a Kistler Charge Conditioner Type 5010A (not shown) and Scientific Atlanta Model SD-390 Signal Analyzer (not shown).

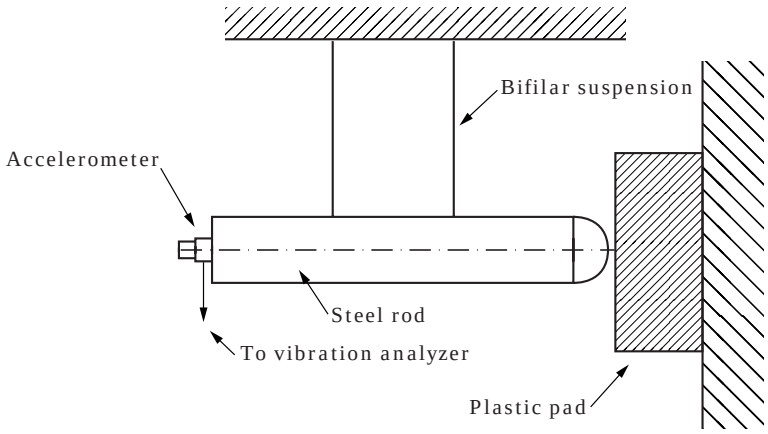

Figure 7. Experimental rig for study of viscoelastic impact.

The following characteristic moments of impact, such as time to peak acceleration and duration of the impact, were measured as $\vartheta = 1{\cdot}54$ ms and $\alpha = 3{\cdot}83$ ms. Expressions (5) and (7) were then considered as a set of transcendental equations in the unknowns ω and ξ and knowns α and ϑ. Dividing equation (5) by equation (7) one can eliminate the parameter ω:

$$\frac{\alpha}{\vartheta} = \left(\operatorname{atan}\frac{2\xi\sqrt{1-\xi^2}}{1-2\xi^2}\right)\Big/\left(\operatorname{atan}\frac{(4\xi^2-1)\sqrt{1-\xi^2}}{\xi(3-4\xi^2)}\right). \tag{15}$$

By first solving equation (15) for ξ and second equation (5) for ω it was estimated that $\xi = 0{\cdot}14$, $\omega = 755$ rad/s. The expression for acceleration from equation (4) was evaluated further with the identified parameters ω and ξ. The time history of acceleration development was generated numerically. The initially unknown

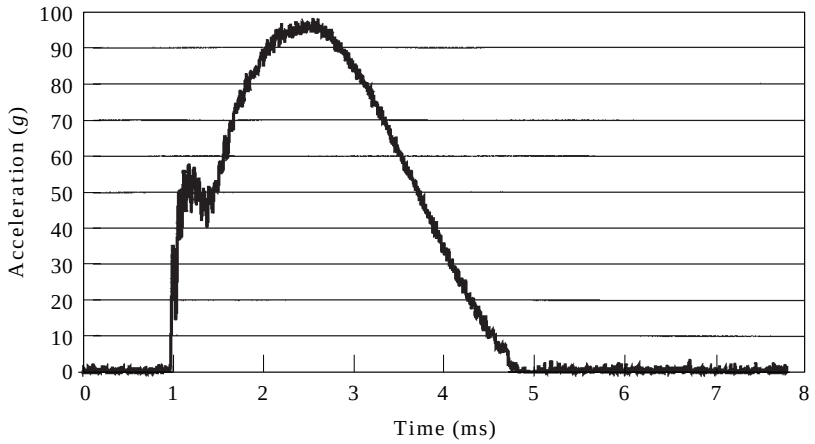

Figure 8. Sample of the time history of acceleration at viscoelastic impact.

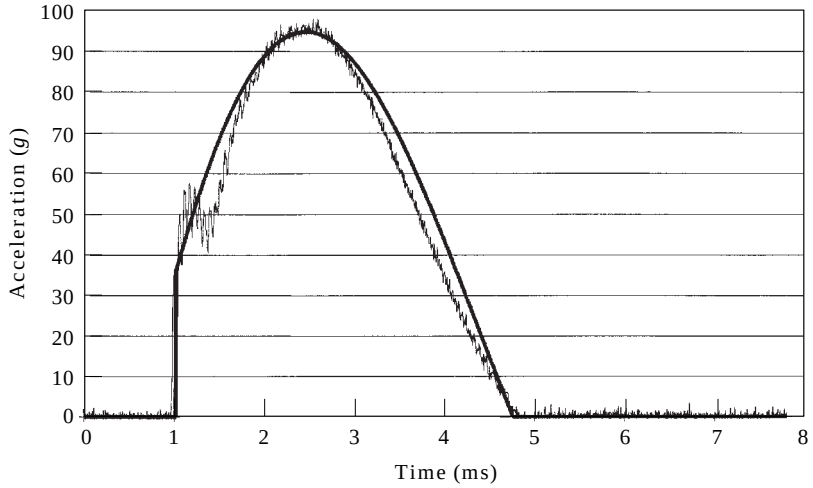

Figure 9. Experimental (——) and analytical (—) time histories of acceleration at viscoelastic impact.

approaching velocity V was estimated by means of a least squares method. For this certain case, $V = 1{\cdot}45$ m/s was obtained. Figure 9 depicts superimposed and practically coinciding time histories of acceleration at impact obtained in the experiment and that obtained theoretically.

4. MODEL OF BUMPERED VIBRATION ISOLATOR

4.1. THEORETICAL CONSIDERATIONS

Figure 10 depicts schematically a machine of total mass M supported by a resilient element represented as a parallel combination of spring K and of dashpot

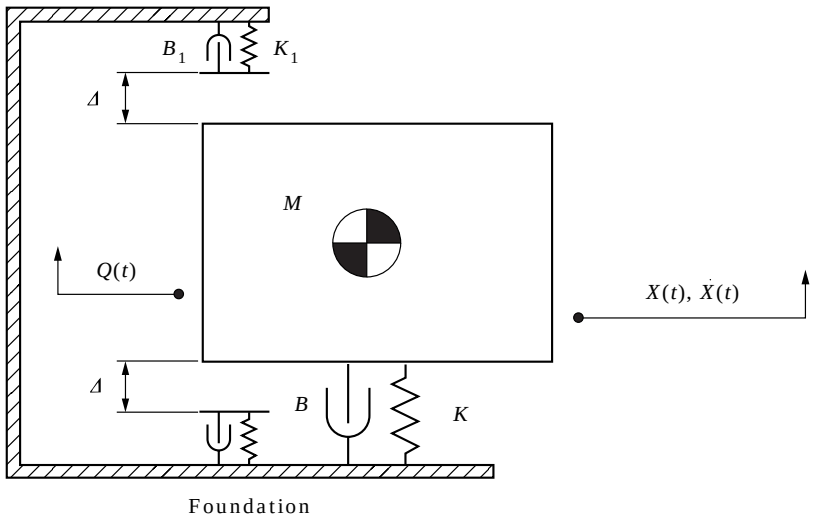

Figure 10. Mechanical model of bumpered vibration isolator.

B. Machine vibration is originated by a dynamic force $Q(t)$. In the case of machine kinematic excitation by an acceleration $A(t)$ the dynamic force will be considered as a translational force of inertia $Q(t) = -A(t)M$.

The deflection $X(t)$ is limited symmetrically by the visco-elastic bumpers modelled as a parallel combination of a spring K_1 and of a dashpot B_1 (see section 2 above). The bumpers were installed over the same foundation symmetrically with respect to the position of static equilibrium of the vibration isolator. The value of the sway space (clearance) is denoted by Δ: see Figure 10.

The differential equation of the motion of the entire system with respect to collisions may be obtained in the form

$$M\ddot{X} + B\dot{X} + KX + \Phi(X, \dot{X}) = Q(t), \tag{16}$$

where $\ddot{X}$, $\dot{X}$ are machine acceleration and velocity, respectively; $\Phi(X, \dot{X})$ is the threshold-type force of impact [3],

$$\Phi(X, \dot{X}) =$$

$$\left\{\begin{array}{ccc} K_1(|X| - \Delta) + B_1\dot{X} & \forall & [X \geqslant \Delta \wedge \Phi(X, \dot{X}) > 0 \vee X \leqslant -\Delta \wedge \Phi(X, \dot{X}) < 0] \\ 0 & \forall & [X \geqslant \Delta \wedge \Phi(X, \dot{X}) < 0 \vee X \leqslant -\Delta \wedge \Phi(X, \dot{X}) > 0] \\ 0 & \forall & |X| \leqslant \Delta \end{array}\right\}. \tag{17}$$

Dividing both parts of equation (16) by M yields

$$\ddot{X} + 2\xi\Omega\dot{X} + \Omega^2 X + f(X, \dot{X}) = Q(t)/M, \tag{18}$$

where the following notations are used:

$$\omega^2 = \frac{K}{M}, \qquad \bar{\omega} = \frac{\omega}{2\pi}, \qquad \xi = \frac{B}{2M\omega}, \qquad \omega_1 = \frac{K_1}{M}, \qquad \bar{\omega}_1 = \frac{\omega_1}{2\pi}, \qquad \xi_1 = \frac{B_1}{2M\omega_1},$$

$$f(X, \dot{X}) =$$

$$\left\{\begin{array}{ccc} \omega_1^2(|X| - \Delta) + 2\xi_1\Omega_1\dot{X} & \forall & |X| \geqslant \Delta \wedge \{[\operatorname{sgn} f(X, \dot{X})][\operatorname{sgn}(X)]\} > 0 \\ 0 & \forall & |X| \geqslant \Delta \wedge \{[\operatorname{sgn} f(X, \dot{X})][\operatorname{sgn}(X)]\} < 0 \\ 0 & \forall & |X| < \Delta \end{array}\right\}. \tag{19}$$

Here the parameters ω and ξ define the undamped natural frequency and loss factor of linear vibration isolator, ω_1 and ξ_1 are the apparent undamped natural frequency and loss factor of the bumper related to the mass of the machine. The notations $\bar{\omega}$ and $\bar{\omega}_1$ denote corresponding natural frequencies expressed in Hz.

The intergation of equation (18) with the force of impact of equation (19) was carried out in a MatLab/Simulink computational environment by using the fifth-order Dormand-Prince method with variable time steps. The Simulink model is represented in Figure 11. In accordance with the MIL-810E as applied for the specific gimballed electro-optical device, the vibration isolator was subjected to the standard vibration inputs: classical saw-tooth shock $50g$ @ 18 ms and broadband random excitation with overall level of $16{\cdot}6g$ RMS (see Figure 15(c) of section 4.4).

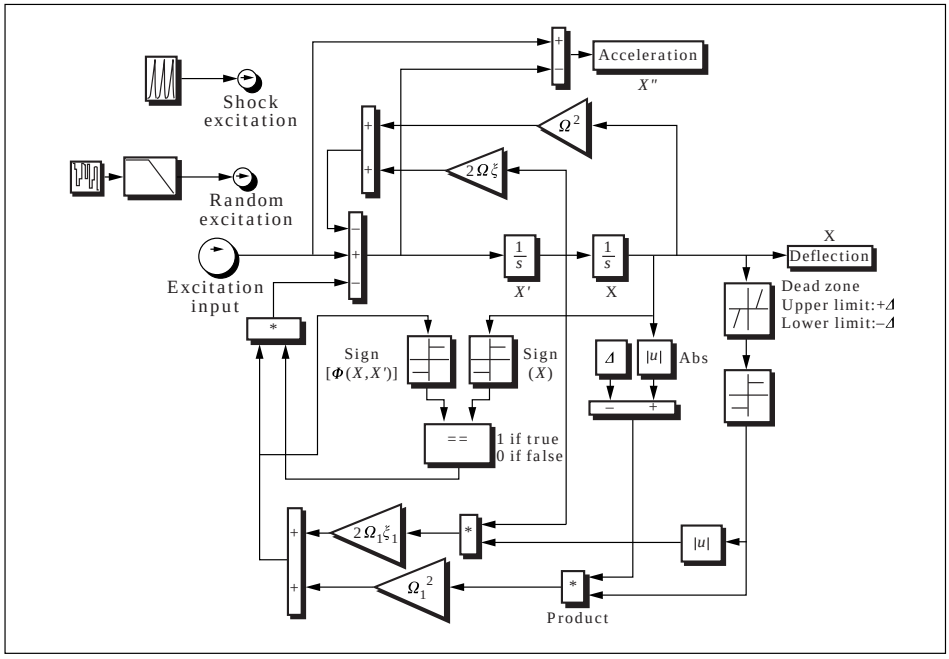

Figure 11. Simulink model of bumpered vibration isolator.

4.2. OPTIMIZATION OF VIBRATION ISOLATOR

The typical problem of the optimization of robust vibration isolator with respect to space limitation, resilient support and flexible interface integrity is to minimize peak acceleration at the permitted peak deflection.

In a very common case, the solution of this problem requires numerous simulations of the model in Figure 11 with application of an optimization procedure.

In order to simplify the solution of this primary optimization problem we will introduce into the consideration the criterion of quality of the vibration isolator (as discussed previously in section 3). It is the product of the peak values of acceleration and deflection obtained in the same test.

The single collision of a solid free body with viscoelastic bumper was studied analytically in section 3. It was shown that there exists a minimum of the above criterion with respect to bumper loss factor. The optimal value of the loss factor of the bumper appeared to be 0·4 independently of the other parameters of the model, such as approaching velocity and stiffness of the bumper.

The results of this analysis cannot be applied directly for the case of arbitrary excitation. Nevertheless, one could expect some sort of similarity with respect to the existence of such an optimum. Moreover, for the undamped and low-frequency vibration isolator such a minimum has to be located close to that obtained for the free body.

4.3. CLASSICAL SAW-TOOTH SHOCK TEST

The model in Figure 11 was subjected to the classical saw-tooth shock of acceleration 50g @ 18 ms. The invariable parameters of the model were as follows: $\bar{\omega} = 15$ Hz, $\xi = 0{\cdot}05$, $\Delta = 0{\cdot}0015$ m. The variables $\bar{\omega}_1$ and ξ_1 were varied within the ranges $\bar{\omega}_1 \in [80, 200]$ Hz with a step of 10 Hz and $\xi_1 \in [0, 1]$ with a step of 0·1. At each simulation, the product of the peak values of acceleration and deflection (signified as Π) was saved and the corresponding set of 12 curves $\Pi = \Pi(\xi_1)$ at different $\bar{\omega}_1$ were put together. The curves obtained, when plotted on the same graph, were located very close to one another. The corresponding minimum of each curve was located in the close neighbourhood of the point $\xi_1 = 0{\cdot}4$. Figure 12(a) represents the averaged curve $\Pi(\xi_1)$ with standard deviation error bars superimposed. Thereby, our suggestion about the existence of a general optimum with respect to bumper loss factor was confirmed.

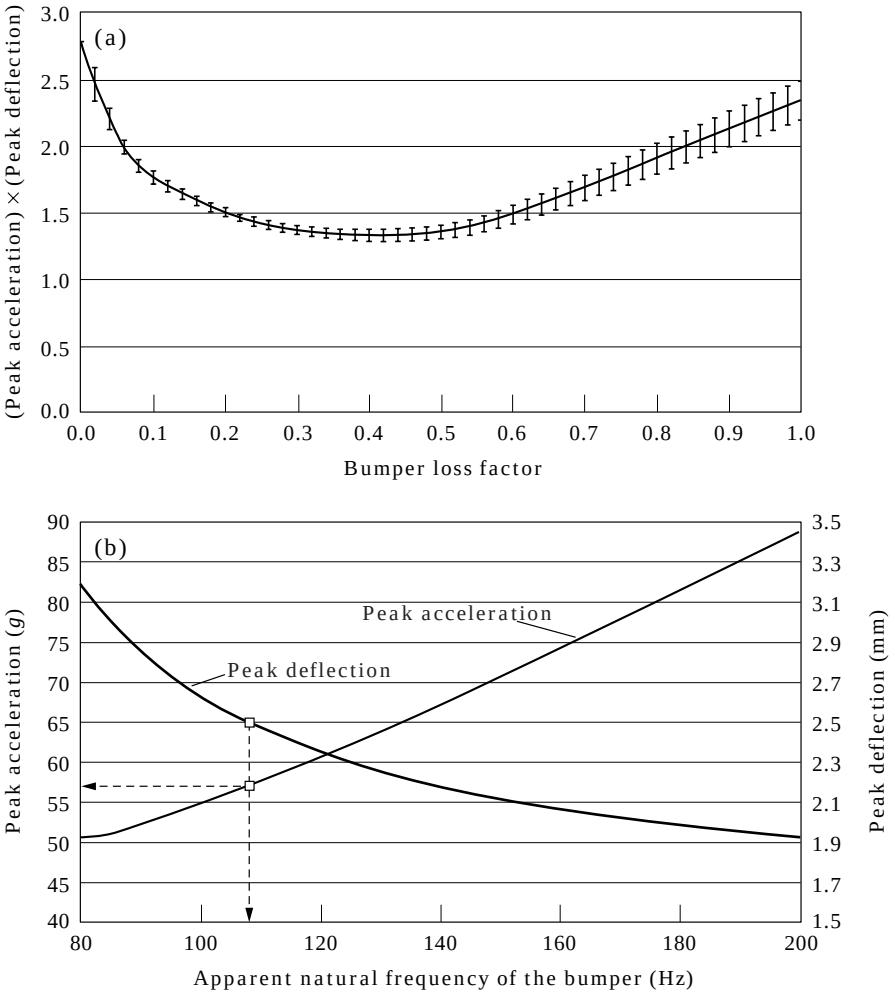

Figure 12. Optimization and choice of vibration isolator for shock test.

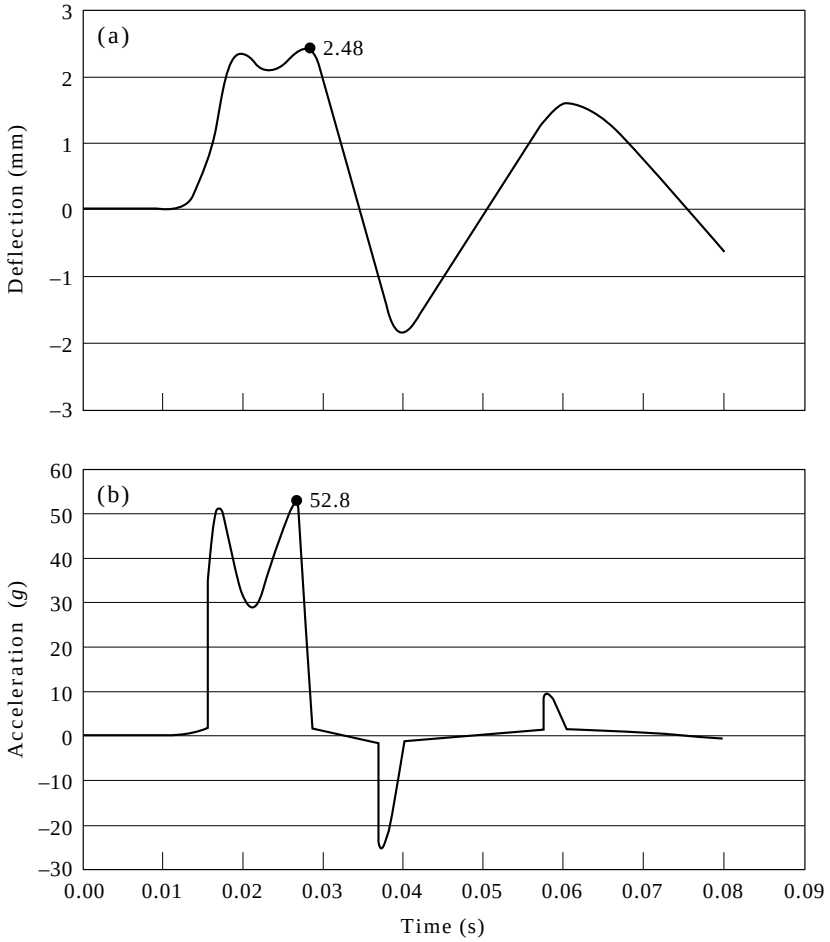

Figure 13. Deflection (a) and acceleration (b) time histories of optimized vibration isolator for shock test.

The further solution of a primary optimal problem is carried out with the fixed value of bumper loss factor $\xi_1 = 0{\cdot}4$. Figure 12(b) depicts superimposed curves representing the peak values of acceleration and deflection as functions of apparent natural frequency of the bumper at a fixed loss factor 0·4. This figure may be treated as a diagram for the choice of bumper stiffness at permitted peak deflection of the vibration isolator. If, for example, it was defined by design the maximum deflection of 2·5 mm, then the apparent natural frequency of the bumper of 108 Hz has to be chosen. As a result of this choice the peak acceleration will be about 54*g* (see Figure 12(a)). Figures 13(a, b) represent the corresponding simulated time histories for the deflection and acceleration with labelled peak values.

In the same manner, the inverse optimization problem for a vibration isolator may be solved. By setting any desirable value of peak acceleration, the necessary stiffness of the bumper may be chosen and the peak deflection of the vibration isolator may then be estimated.

4.4. WIDEBAND RANDOM EXCITATION TEST

The model of Figure 11 was subjected to the wideband random vibration with total level of 16·6g RMS. The PSD spectra of the excitation is presented in Figure 15(c). As in the case of shock excitation, the invariable parameters of the model were $\bar{\omega} = 15$ Hz, $\xi = 0{\cdot}05$ and $\Delta = 0{\cdot}0015$ m. The variables $\bar{\omega}_1$ and ξ_1 were subjected to variation within the ranges $\bar{\omega}_1 \in [80, 200]$ Hz with a step of 10 Hz and $\xi_1 \in [0, 1]$ with a step of 0·1. At each simulation the product of the peak values of acceleration and deflection (signified as Π) was saved and the corresponding 12 functions $\Pi = \Pi(\xi_1)$ at different $\bar{\omega}_1$ were put together. Similarly to those obtained previously, the mentioned curves were located very close to one another and the corresponding minimum of each curve was located in the close neighbourhood of the point $\xi_1 = 0{\cdot}4$. Figure 14(a) represents the averaged curve $\Pi(\xi_1)$ with standard deviation error bars superimposed. Thereby, the suggestion about the existence of

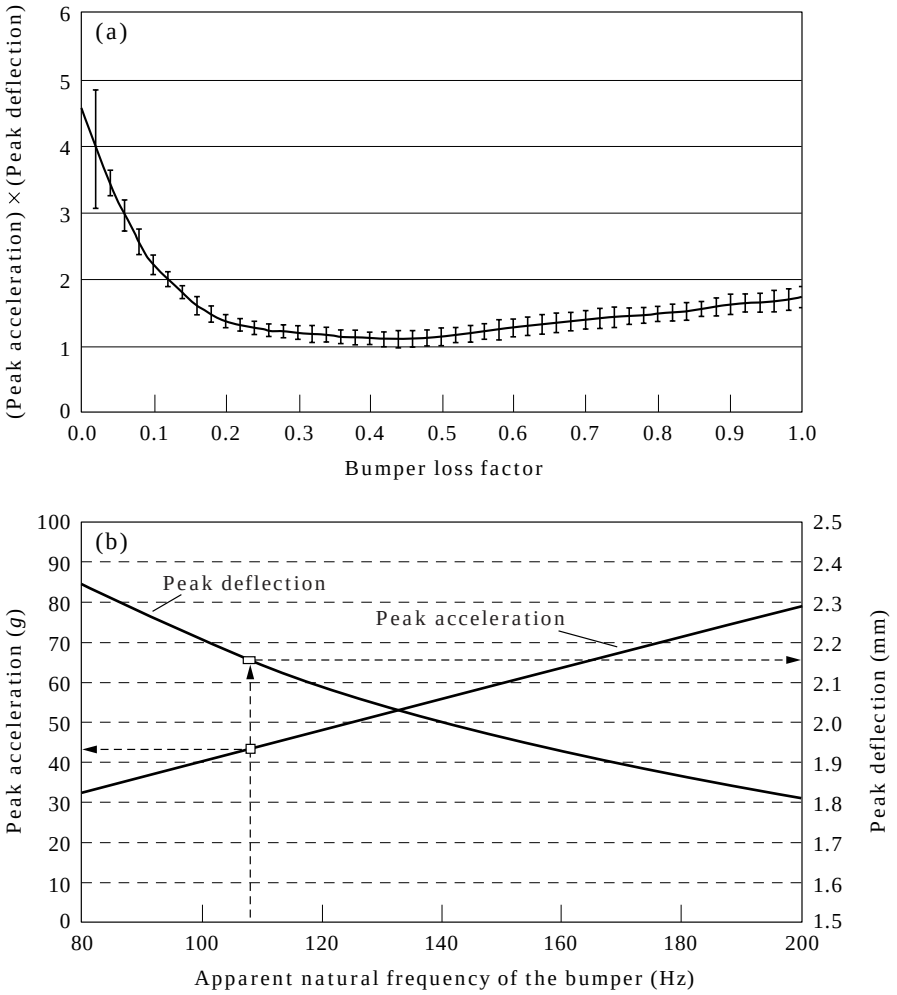

Figure 14. Optimization and choice of vibration isolator for random vibration test.

a general optimum with respect to bumper loss factor was confirmed even in the more complex case of wideband random excitation.

Further solution of a primary optimal problem may be carried out for the fixed value of bumper loss factor of $\xi_1 = 0{\cdot}4$. Figure 14(b) presents the superimposed curves of peak values of acceleration and of deflection under wideband random vibration as a function of apparent natural frequency of the bumper. The figure may be treated as an independent diagram for the choice of bumper stiffness for permitted peak deflection of the vibration isolator under wideband random vibration.

From Figure 14(b) the peak deflection at wideband random test does not exceed the previously specified level of 2·5 mm. Therefore, the value of apparent natural frequency of the bumper of 108 Hz, which was considered as optimal for the shock test, will be applied for the wideband random test. From Figure 14(b) the peak values of deflection and acceleration will be 2·15 mm and $43g$.

Figure 15 presents the results of simulation of an optimized vibration isolator for a random vibration test. The superimposed fragments of time histories of excitation (dotted line) and of vibration isolator response (solid line) are presented in Figure 15(a). The relatively rare spikes in the vibration isolator response are of a characteristic quasi-periodic impulsive nature with peak values even lower than that of the excitation.

Figure 15(b) depicts the normalized probability density distributions (PDF) of excitation and that of the vibration isolator response. The analysis of the corresponding densities emphasizes the conclusion: the main portion of the response of the vibration isolator is low-powered. It is located mainly in a centred narrow area of $\pm 2g$; the distribution tails (embodying the high levels of acceleration) are much lower than that of the excitation.

Figure 15(c) presents the superimposed graphs of power spectral densities (PSD) of excitation and of vibration isolator response. It illustrates the vibration attenuation in a wide high-frequency range of 100–2000 Hz. In fact, the overall level (OA) of vibration was attenuated up to $7{\cdot}7g$ RMS as compared with $16{\cdot}6g$ RMS of the excitation.

From Figure 15(c) only a narrow frequency band located to the right of the linear natural frequency represents certain amplification. Because of system non-linearity, the curve of the apparent transfer function is slightly distorted. It presents a maximum of 2·4 at 35 Hz instead of 15 Hz (natural frequency of the linear system); see the graph of the apparent transfer function in Figure 15(d). Such an amplification ratio is typical for linear heavily damped vibration isolator with a loss factor of about 0·3.

4.5. DYNAMIC SAFETY TEST

As was shown above in section 2, the designed vibration isolator can attenuate the self-induced force exported from the machine to its foundation by a factor of ~ 14. At the same time, the optimally designed bumpers are capable of guaranteeing a soft trim of excessive motions in the case of intensive ambient disturbances, as discussed previously.

It is known from references [2, 3] that vibro-impact resonance in a frequency range located well above the system's linear natural frequency may arise after casual vibration disturbance or frequency pulling at machine start-up. Because of this fact, an additional and absolutely necessary feature of a bumpered vibration protection arrangement is the ability to suppress the vibro-impact resonance for any initial conditions. For this purpose, an additional simulation test was carried out.

In the *dynamic safety* test the dynamic response of the bumpered vibration isolator under intensive disturbance was simulated. The test parameters were: self-induced force 14 N RMS @ 60 Hz and as an external disturbance a classical saw-tooth shock 50*g* @ 18 ms. This test was provided with the apparent natural frequency of the bumper 108 Hz and loss factor 0·4. Figure 16 represents the *safe*

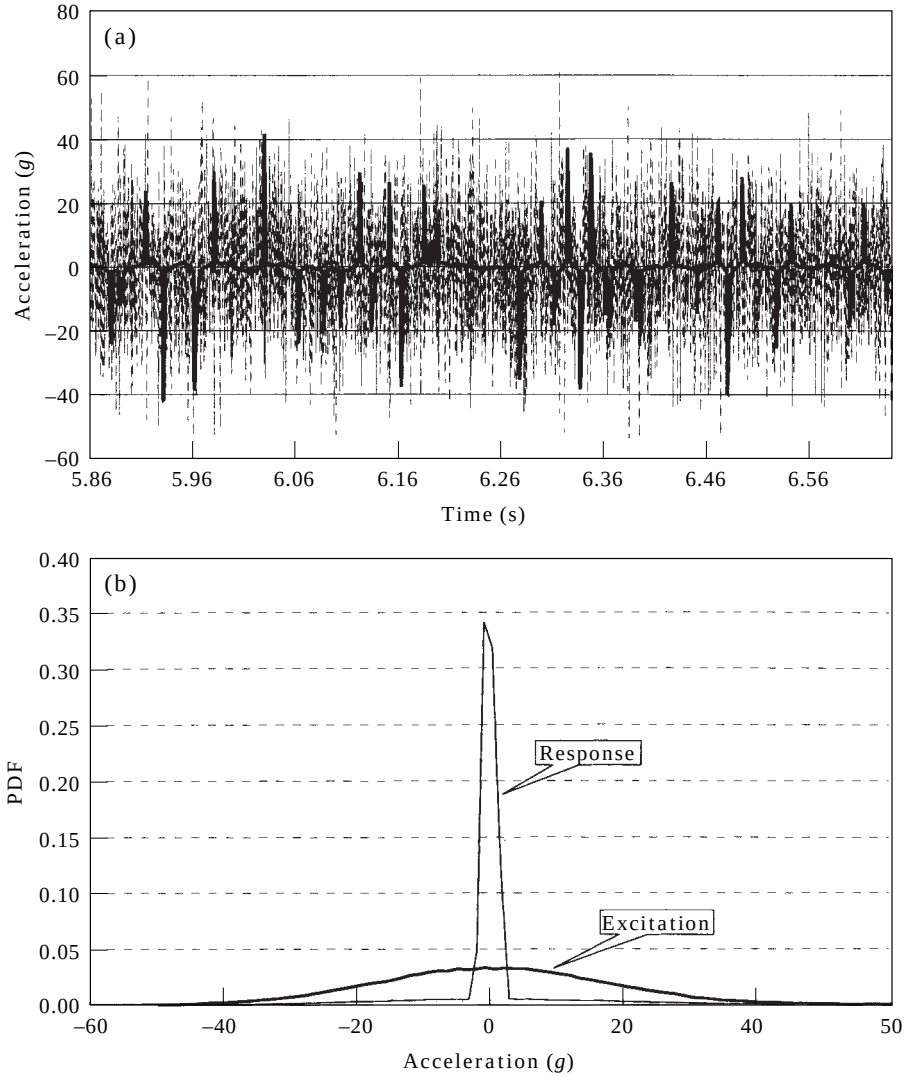

Fig. 15.

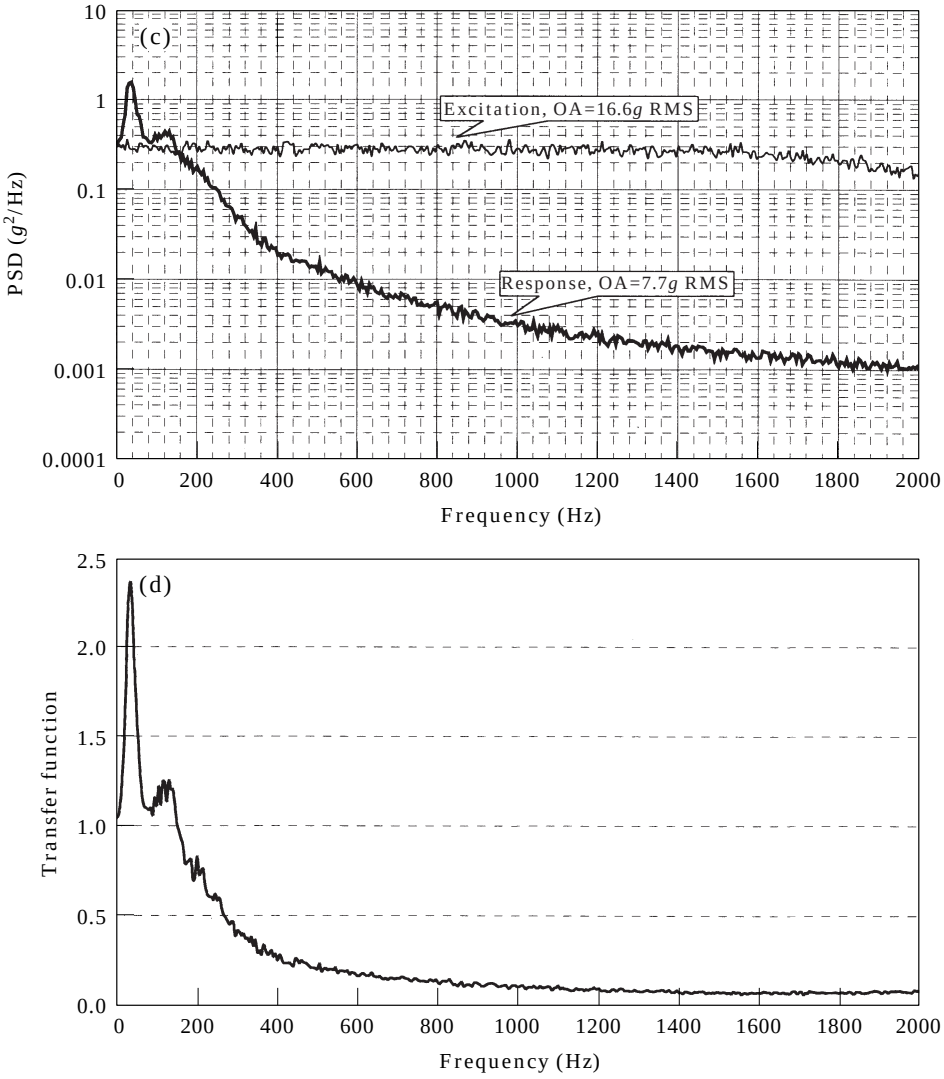

Figure 15. Optimized vibration isolator for random vibration test.

transient response to the vibration isolator on the shock application at the time 0·2 s.

5. EXPERIMENTAL TESTING

The principles of the bumpered vibration isolator were utilized in the design of the vibration protection arrangement for a Ricor model K529H cryocooler, as discussed above in section 2. The characteristic parameters of the applied bumpers were identified through the shock test (similarly to the test described above in section 3) as $\bar{\omega}_1 \approx 110$ Hz and $\xi_1 \approx 0{\cdot}42$ at 23°C.

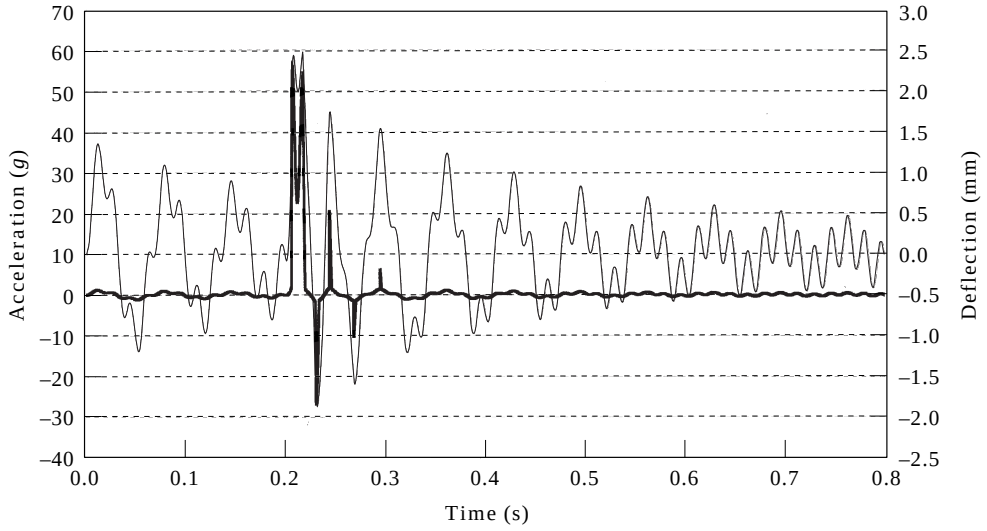

Figure 16. Simulated transient response of the vibration isolator for dynamic safety test. ——, Acceleration; ——, deflection.

Figure 17 depicts schematically the experimental rig. The intermediate frame of a sprung suspended linear compressor was mounted over the slip table of an *Unholtz-Dickie* vibration exciter Type UD-4. The *Brüel & Kjaer* miniature accelerometer Type 4393 1 was glued to the compressor housing, thus, the axial compressor acceleration was measured. After the charge amplifier 3 the acceleration signal was fed to the vibration analyzer. The second (control) accelerometer 2 was glued to the compressor frame. Its signal after the charge conditioner 4 was fed to the vibration analyzer and to the input of the *Unholtz-Dickie* Type 5200 vibration controller, operating in a closed-loop mode. The saw-tooth shock, random vibration and dynamic safety tests were carried out.

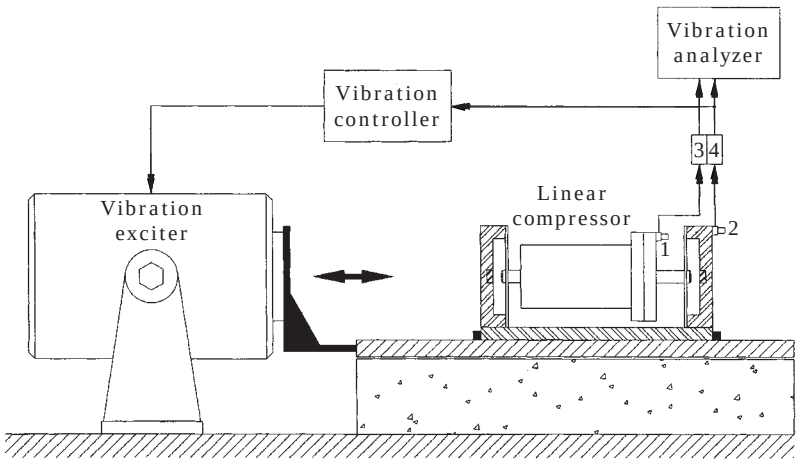

Figure 17. Experimental rig.

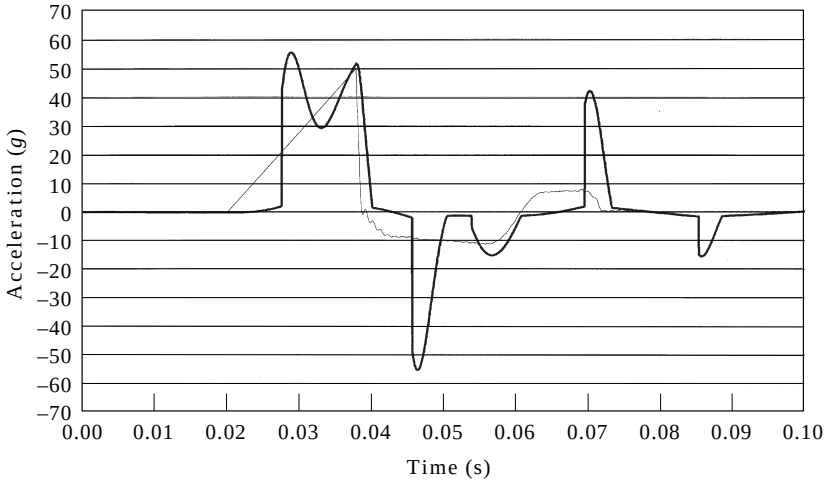

Figure 18. Time histories of excitation (——) and of vibration isolator response (——) for shock test.

The non-operating compressor unit was exposed to the classical saw-tooth shock test $50g$ @ 18 ms. Figure 18 depicts the superimposed acceleration time histories of the control point and of the compressor housing. The peak acceleration of the primary shock was measured as $55{\cdot}6g$ (compare with $52{\cdot}8g$ obtained in simulation; see Figure 13). The few secondary intensive collisions occurred as a result of the operation of the vibration controller performing the fast return of the exciter table to the initial position.

The compressor unit was exposed to random kinematic excitation (uniform acceleration PSD value of $0{\cdot}3g^2$/Hz from 20 to 1000 Hz and a further decline to $0{\cdot}05g^2$/Hz at 2000 Hz; overall RMS value $16{\cdot}4g$; see Figure 19(b)).

The vibration analyzer registered the time histories of the control point and of the compressor unit accelerations. Figure 19(a) depicts fragments of corresponding samples superimposed. Similarly as in the simulation, the relatively rare, low peaks in the compressor response (solid line) (compared with the acceleration excitation (dotted line)) are of characteristic quasi-periodic impact nature with peak values lower than that of the excitation.

By using 75% overlapping, *Hanning* weighting, 2048 point FFT and exponential averaging the corresponding 800-lines PSD spectra were obtained. Figure 19(b) (semilog-Y scaling is used) depicts the superimposed PSD spectra for the control point and for the compressor. Similarly as in the simulation (see Figure 15(c)), the experiment demonstrates vibration attenuation in a wide high-frequency span of 100–2000 Hz. As a matter of fact, the overall level (OA) of vibration was attenuated up to $7{\cdot}5g$ RMS as compared with $16{\cdot}4g$ RMS of the excitation.

The apparent transfer function of Figure 19(c) displayed a maximum level of $\sim 2{\cdot}3$ at a frequency of ~ 36 Hz; that is characteristic for the linear vibration isolator with the loss factor of 0·3; the shift of the resonance frequency was due to the vibration isolator non-linearity; see the discussion of the previous section.

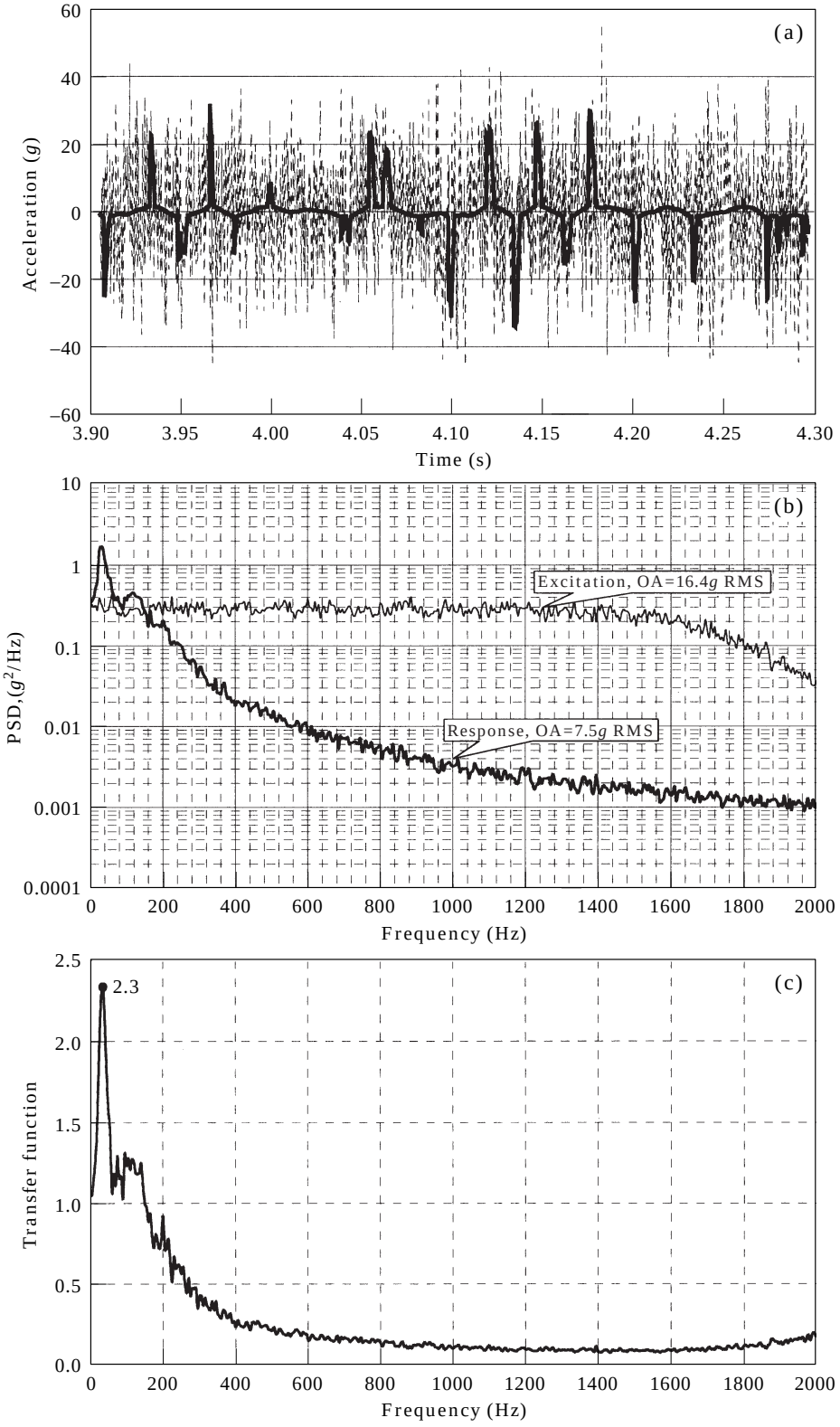

Figure 19. Vibration isolator dynamics for random vibration test.

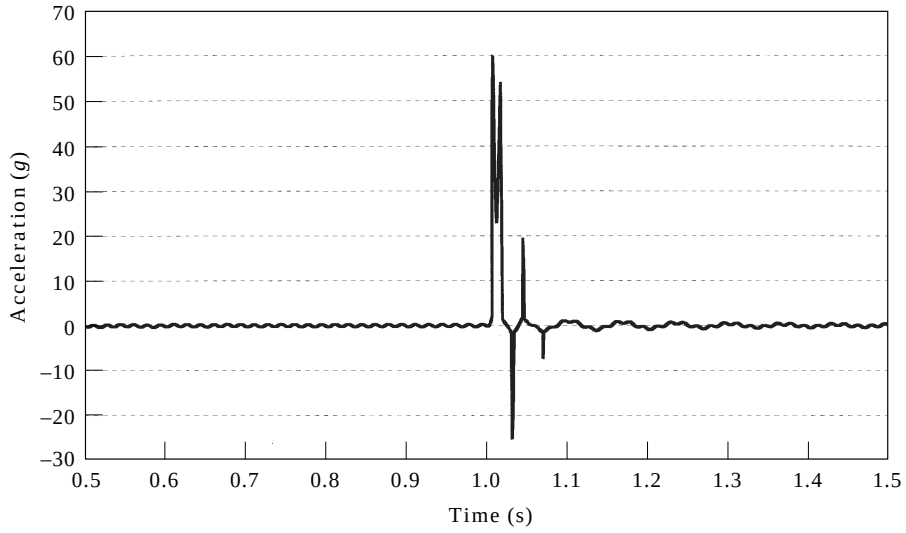

Figure 20. Vibration isolator for dynamic safety test.

The aim of the dynamic safety test was to check the operating system's ability to withstand intense shock without a vibro-impact resonance arising.

The operating cryocooler was mounted upon the vibration exciter table and exposed to a saw-tooth kinematic shock 50*g* @ 18 ms. Figure 20 depicts the time history of the compressor unit acceleration. Before the shock application, the compressor unit steady state amplitude of acceleration was about 0·45*g*. As a result of shock application, a few intensive collisions over the bumpers occurred with sequential "positive" and "negative" acceleration peaks. After a finite number of further low powered collisions the transient vibroimpact process was over and initial impactless steady operation of the compressor unit was re-established. The same test was repeated for each possible compressor orientation. Even in the case of asymmetrical bumper locations due to the action of gravitational forces, safe transients were obtained.

6. CONCLUSIONS

The tested bumpered vibration isolation arrangement of a Ricor model K529H linear compressor provided the following: 93% vibration isolation of the fundamental component of the self-induced force; safe and soft trim of excessive dynamic deflections.

The Ricor K529H cryocooler met the requirement of low self-induced force export and passed the full programme of shock and broadband random vibration environmental testing in accordance with MIL STD-810E without degradation in performance.

REFERENCES

1. C. M. Harris and C. E. Crede (editors) 1961 *Shock and Vibration Handbook*. New York: McGraw-Hill Book Company.
2. M. Z. Kolovsky 1966 *Non-linear Theory of Vibration Protection Systems*. Moscow: Nauka (in Russian).
3. V. I. Babitsky 1998 *Theory of Vibro-Impact Systems with Applications*. Berlin: Springer-Verlag. Revised translation from Russian. Moscow: Nauka, 1978.
4. A. M. Veprik, A. Meromi and A. Leschecz 1997 *Proceedings of SPIE* 11*th Annual International Symposium on Aerospace/Defense Sensing*, *Simulation and Controls* "*AeroSense*", *Orlando*, *FL*, Volume 3061 *Infrared Technology and Applications XXIII*, 640. Novel technique of vibration control for split Sterling cyrocooler with linear compressor.
5. L. L. Beranek 1971 *Noise and Vibration Control*. New York: McGraw-Hill Book Company.